Three possible types of coronagraphs for the E-ELT PCS instrument

Alexis Carlotti[a], Mamadou N'Diaye[b], Laurent Pueyo[b], and Dimitri Mawet[c]

[a]CNRS, IPAG, F-38000 Grenoble, France
[b]STScI, 3700 San Martin Drive, Baltimore, MD 21218, USA
[c]ESO, Alonso de Cordova 3107, Vitacura, Santiago, Chile

ABSTRACT

The spectral characterization in the near infrared of Neptune-like planets and super-Earths is one of the main science objectives of the E-ELT. The planetary camera and spectrograph (PCS) will be in charge of making it possible. We have designed three different instruments: pure apodizers, apodized Lyot coronagraphs, and apodized vortex coronagraphs. In each cases the central obscuration and the secondary supports are taken into account in the design of the apodizer. We present a trade study of the imaging performance of these coronagraphs, and we describe how sensitive these coronagraphs are to various aberrations. This is used to assess the potential complementarity between these three types of instruments. Finally, we also consider the feasibility of an active control of aperture discontinuities and/or a phase induced amplitude apodization using the two deformable mirrors of an extreme adaptive optics system associated with the coronagraphs.

Keywords: High-contrast imaging, coronagraphy, exoplanets, apodization

1. INTRODUCTION

The first light of the European extremely large telescope (E-ELT) is expected for 2022. When it is built, this 39m telescope will be the largest, single aperture, optical telescope in the world. The direct detection and characterization of exoplanets is one of the main scientific objectives that will be tackled by the instruments of the E-ELT. The two first light instruments - HARMONI and MICADO - are likely to possess a coronagraphic mode, which they will use to characterize Jupiter-like planets in the near-infrared. The METIS instrument will conduct similar observations in the mid-infrared. Because they will only rely on the adaptive optics of the telescope itself, these three instruments will be limited to 10^{-6} contrast.

On the contrary, the planetary camera and spectrograph (PCS) will use a dedicated adaptive optics system. It is expected that PCS will characterize planets with a $10^{-9} - 10^{-8}$ contrast with their host star. In addition to Jupiter-like planets, it will study Neptune-like planets and super-Earths. In the H-band, the large diameter if this telescope could potentially make it possible to achieve 15mas angular separations with a coronagraph, and this would be enough to directly detect and characterize rocky planets around M-dwarfs.[1]

Two main obstacles prevent direct imaging: the diffraction effects due to the finite size of the telescope, and the wavefront aberrations introduced when light goes through the atmosphere and the optics of the telescope and the instrument.

Adaptive optics is used to correct for wavefront aberrations, and the diffraction effects can be dealt with a coronagraph by either (a) remodeling the point-spread function of the telescope by modifying the energy density and/or the phase in the pupil plane, (b) destructively interfering the light of the star with itself, or (c) doing a combination of both.

Designing coronagraphs for arbitrary apertures has become mandatory as the scientific objectives have become more ambitious in term of contrast and separation, and the apertures of several near-future telescope such as WFIRST-AFTA or E-ELT have a strong central obscuration and spiders structure, creating more artifacts in

Further author information: (Send correspondence to Alexis Carlotti)
Alexis Carlotti: E-mail: alexis.carlotti@obs.ujf-grenoble.fr, Telephone: +33 476 514 521

Ground-based and Airborne Instrumentation for Astronomy V, edited by Suzanne K. Ramsay, Ian S. McLean, Hideki Takami, Proc. of SPIE Vol. 9147, 91479D · © 2014 SPIE · CCC code: 0277-786X/14/$18 · doi: 10.1117/12.2056842

the point-spread function (PSF) which becomes less friendly for high-contrast imaging. This paper describes the possible design of apodized coronagraphs for the E-ELT, in particular for the PCS instrument.

Apodizers can be designed for arbitrary apertures to shape the PSF of the telescope to either (a) create high-contrast directly,[2,3] or (b) allow a coronagraph to create high-contrast in spite of the complex features in the aperture. An apodizer can be designed to work with a Lyot coronagraph, forming an apodized Lyot coronagraph[4,5] (APLC), or other focal plane masks such as a four-quadrant phase mask[6,7] (4QPM), or a vortex phase mask.[8–10]

In each case the optimization process of the apodizer is similar. The apodizer is represented by an N-by-N array, and an apodization coefficient $a_{i,j}$ is associated to every element of the array. The total transmission $\sum_{i=1}^{N}\sum_{j=1}^{N} a_{i,j}$ is maximized, while constraints are set on the real and imaginary parts (or the intensity) of a linear transform of the apodizer, as seen behind the aperture. Constraints will not be set in every point of the second optical plane, but only in those of interest.

This linear transform will depend on the type of coronagraph that is considered: if the apodizer directly creates high-contrast, the linear transform will be a Fourier transform, and if the apodizer creates high-contrast when associated with a coronagraph, the linear transform will be a convolution of the apodizer and a function that will represent the action of the coronagraph.

For the first type of instrument the region of interest in which the amplitude or the intensity of the electric field is constrained is the discovery space in the image plane. For the second type of instrument, the region of interest can either be the discovery space in the final, second image plane, or the region of the Lyot plane that is defined by the Lyot stop.

In these optimizations, the size of the image planes is finite, whether this is explicitly or implicitly stated. The finite size of the image plane makes the apodizer transmission binary.[3,11] This allows the apodizer to be manufactured using photolithography, in the same way the microdots apodizers have been manufactured for the APLC of the GPI and the SPHERE instruments.[12–14] Because of this property, these apodizers can rightfully be called shaped pupils.

In this paper we consider three types of apodized coronagraphs that we design for the aperture of the E-ELT:

1. SP: Shaped pupils to directly create high-contrast.
2. SPLC: Shaped pupils to create high-contrast with a Lyot mask and a Lyot stop.
3. AVC: Shaped pupils to create high-contrast with a vortex mask and a Lyot stop.

Because of their optical design, we expect these coronagraphs to have different properties, in particular regarding to their sensitivity to low-order aberrations and to bandwidth. Trade-offs exist between these sensitivity properties and the ideal performance of the coronagraphs (such as throughput, inner working angle and contrast).

The purpose of this paper is to characterize the ideal performance of these three types of coronagraphs, while also characterizing their sensitivity to low-order aberrations. Once characterized, these three approaches to high-contrast imaging can be compared.

Sec.2 details the properties of the SP, SPLC, and AVC. Sec.3 presents a sensitivity analysis in broadband for the SP and SPLC, and in monochromatic light for the AVC. Sec.4 discusses the complementarities and main differences between these coronagraphs. Sec.5 draws a conclusion to the paper.

2. THREE TYPES OF APODIZED CORONAGRAPH FOR THE APERTURE OF THE E-ELT

The aperture of the E-ELT is displayed in Fig.1. The outer diameter of the aperture is here limited by a circular edge that effectively limits the diameter to 37m. This is done to work with a circular external edge instead of a saw-shaped edge. The aperture has a 30% central obscuration with 6 spiders in an hexagonal configuration. The spiders are 0.5m thick, making them 1.35% of the pupil diameter.

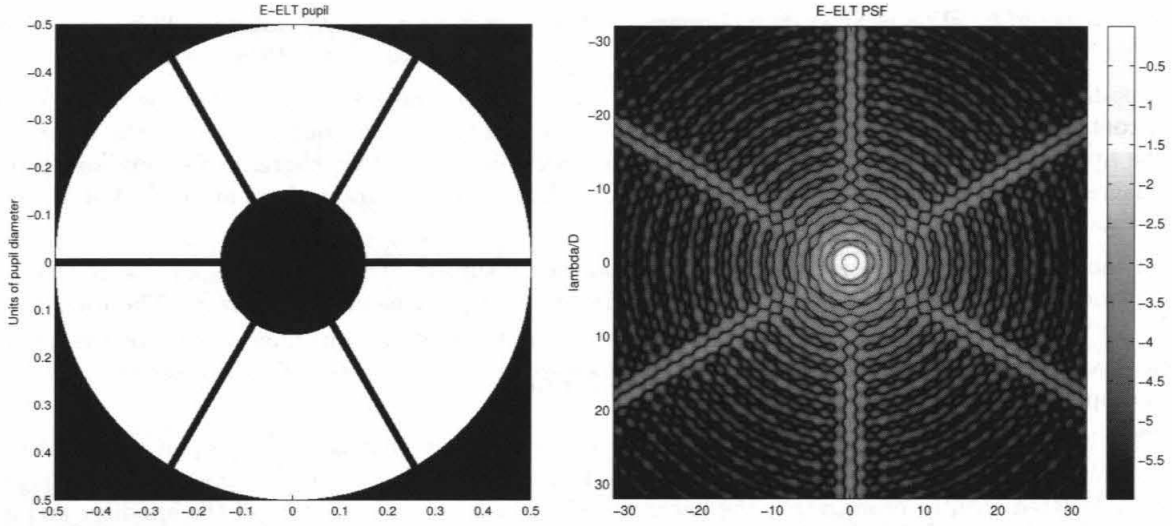

(a) (b)

Figure 1. Aperture (a) and PSF (b) of the E-ELT. Intensity in the image plane is represented in a log scale, and axes are in units of λ/D.

Expected contrast	10^{-6}			
Azymutal extent	2×60 deg.		360 deg.	
Throughput	25%	50%	25%	50%
# of mask	1	2	3	4
IWA (λ/D)	2.9	4.3	5.1	7.0
1^{st} image plane effective contrast	1.5×10^{-6}	8.7×10^{-7}	9.7×10^{-7}	1.2×10^{-6}
2^{nd} image plane effective contrast	4.0×10^{-7}	1.2×10^{-7}	2.2×10^{-7}	2.5×10^{-7}

Table 1. Throughput, IWA, and effective contrast of the four SP coronagraphs (number 1 through 4) optimized for the E-ELT aperture to directly create 10^{-6} contrast. The contrast is measured both in the first image plane - where it is close to the expected contrast for which the mask was designed - and in the second image plane, after the Lyot stop, where it is smaller than the expected contrast. This demonstrates that using a Lyot stop indeed improves the contrast, although the shaped pupils is not explicitly designed for it.

We design the coronagraphs to create 10^{-6} and 10^{-8} contrast at a given distance from the star so that the throughput of the coronagraph is either 25% or 50%. For the shaped pupils, we also consider two types of discovery regions in the image plane: a full 360 degree region, and two symmetric 60 wide degree regions. In the case of the AVC, as it is not possible to set a separation angle, it is also not possible to adjust the throughput of the coronagraph, and the only degree of freedom is the contrast. In total eight SPs, four APLCs, and 2 AVCs have been optimized.

The following three subsections describe the main properties of the 14 coronagraphs. All contrast, IWA, and OWA are given for monochromatic light.

2.1 Shaped pupil coronagraph

The shaped pupils that we have numerically optimized are arrays of 1000-by-1000 points. In practice, however, we have taken advantage of the four fold symmetry of the aperture to restrain the computation to arrays of 500-by-500 points that cover one quadrant of the pupil plane.

Tab.1 and 2 list the properties of the eight SP coronagraphs optimized for a 10^{-6} and a 10^{-8} contrast, respectively. Each of them is associated to a given azymutal extent, and a throughput. We display the IWA of each solution, as well as the contrasts measured in the dark zone in the first and second image planes.

Expected contrast	10^{-8}			
Azymutal extent	2×60 deg.		360 deg.	
Throughput	25%	50%	25%	50%
# of mask	5	6	7	8
IWA (λ/D)	4.0	5.6	6.8	9.0
1^{st} image plane effective contrast	1.5×10^{-8}	1.9×10^{-8}	2.2×10^{-8}	2.6×10^{-8}
2^{nd} image plane effective contrast	4.3×10^{-9}	2.0×10^{-9}	2.0×10^{-9}	2.6×10^{-9}

Table 2. Throughput, IWA, and effective contrast of the four SP coronagraphs (number 5 through 8) optimized for the E-ELT aperture to directly create 10^{-8} contrast. The contrast is measured both in the first image plane and in the second image plane, after the Lyot stop.

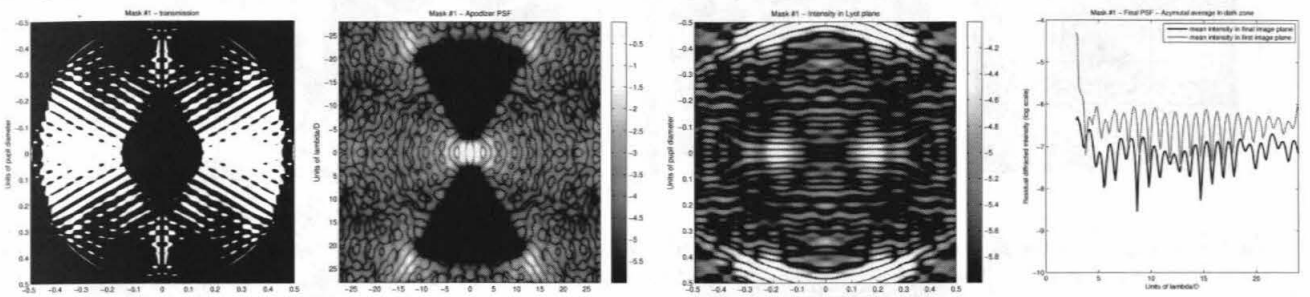

(a) (b) (c) (d)

Figure 2. (a): transmission of mask #1, (b): PSF (first image plane, log scale), (c): residual intensity in Lyot plane (before the Lyot stop has been applied), (d): azymutal average intensity in the first and final image planes (log scale).

Reimaging the image plane behind a Lyot stop helps achieving a significantly lower contrast. For the masks optimized for a 10^{-6} contrast, we observe a 4-7 times lower contrast. For the masks optimized for a 10^{-8} contrast, we observe a 3.5-11 times lower contrast. The effect is stronger for larger IWA.

Unexpectedly, smaller IWA are achieved at the expense of a lower throughput, a higher contrast, or a narrower discovery area. The smallest IWA of the eight masks is found for mask #1, which is showed in Fig.2. Its IWA is 2.9 λ/D, and it corresponds to a 25% throughput coronagraph, a 4.0×10^{-7}-1.5×10^{-6} contrast (measured in the final and first image planes, respectively), and two symmetric 60 deg. wide regions. A lower, 4.3×10^{-9}-10^{-8} contrast results in a $4\lambda/D$ IWA. A higher, 50% throughput results in a $4.3\lambda/D$ IWA. A 360 deg. region results in a 5.1 λ/D IWA. The largest IWA - $9\lambda/D$ - is obtained for a 2.6×10^{-9}-2.6×10^{-8} contrast, a 50% throughput, and a 360 deg. discovery region.

In addition to the transmission of the apodizer; Fig.2 also shows the PSF that it creates, as well as the intensity that remains in the Lyot plane (after the proper focal plane mask has been applied on the PSF). Finally it also shows the remaining diffracted starlight in the final image plane. The same plots are given in

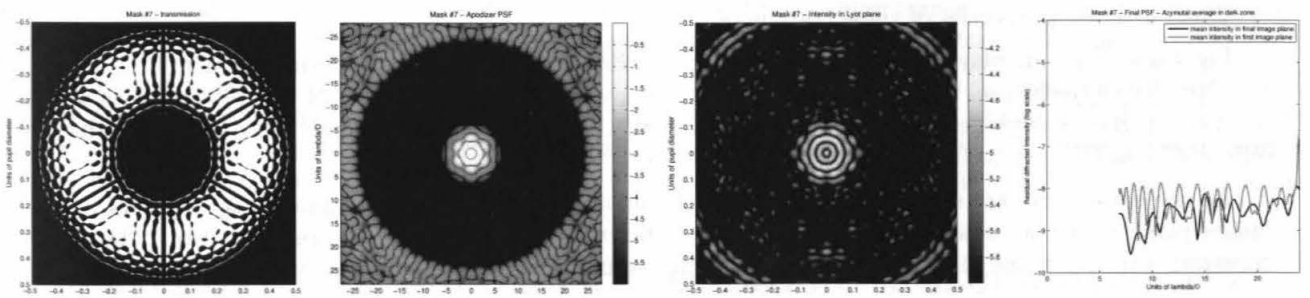

(a) (b) (c) (d)

Figure 3. (a): transmission of mask #7, (b): PSF (first image plane, log scale), (c): residual intensity in Lyot plane (before the Lyot stop has been applied), (d): azymutal average intensity in the first and final image planes (log scale).

Expected contrast	10^{-6}		10^{-8}	
Throughput	25%	50%	25%	50%
# of mask	9	10	11	12
IWA (λ/D)	3.4	6.2	4.3	8.3

Table 3. Throughput, IWA, and effective contrast of the four apodizers (number 9 through 12) optimized for the E-ELT aperture to create 10^{-6} and 10^{-8} contrasts with a Lyot coronagraph formed of a Lyot mask and a Lyot stop. The contrast is measured in the second image plane, after the Lyot stop.

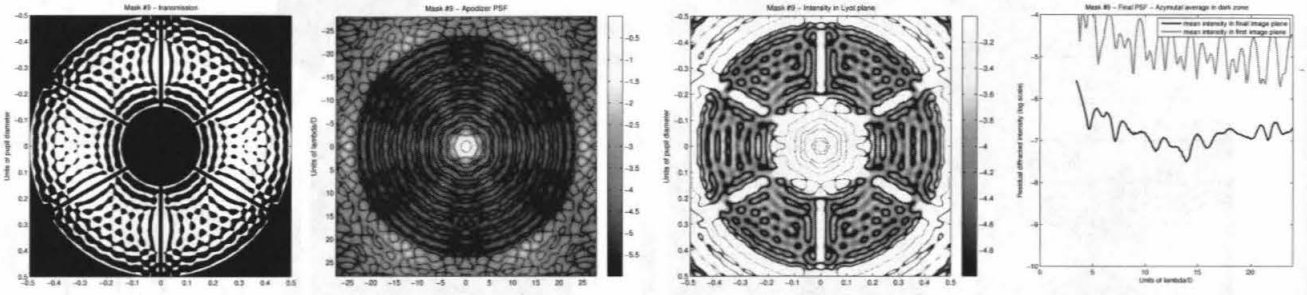

(a) (b) (c) (d)

Figure 4. (a): transmission of mask #9, (b): PSF (first image plane, log scale), (c): residual intensity in Lyot plane (before the Lyot stop has been applied), (d): azymutal average intensity in the first and final image planes (log scale).

Fig.3 for mask #7, which is designed for a 360 deg. region, 10^{-8} contrast.

2.2 Shaped pupil Lyot coronagraph

The four shaped pupils that we have numerically optimized for a Lyot coronagraph have been computed over 512-by-512 points. Here again we have taken advantage of the aperture symmetries to reduce the effective size of the array to 256-by-256, the apodizer being effectively computed over one quadrant of the pupil plane. This number of points is smaller than the one chosen for the SP. This is due to the increased complexity of the computation, which does not go as $N^2 \times M + N \times M^2$ as it is the case with the SP, but as $N^2 \times M^2$.

The computing process for the SPLC is rather similar to the one used for apodized phase mask coronagraphs.[7,10] Instead of a phase mask, however, we assume a Lyot mask in the image plane. The Lyot stop has a central obscuration that is 20% larger than the central obscuration of the E-ELT (about 36% of the pupil diameter). To mitigate diffraction effects due to the finite size of the image plane mask, its outer diameter is 95% of the E-ELT diameter. The spiders thickness has been increased by a factor of two, making them about 3% of the pupil diameter.

As with the apodized phase mask coronagraphs the constraints are set on the intensity of the electric field in the Lyot plane. The properties of the Lyot stop have been adjusted to maximize the throughput of the coronagraph, but they may still be sub-optimal.

Tab.3 lists the properties of these coronagraphs.

Fig.4 and Fig.5 display the transmission of mask #9 and #11, which are designed for a 10^{-6} and a 10^{-8} contrast, respectively, and a 25% throughput. Both figures also display the PSF of the apodizers, as well as the intensity in the Lyot plane, before it has been masked with the Lyot stop. Finally they also show the residual diffracted starlight in the final image plane.

As the constraints are set on the intensity of the on-axis source in the Lyot plane, the contrast in the final image plane is not a constant. A perhaps more efficient way to consider the problem would be to set the constraints in the image plane directly, although this would increase the complexity of the computation.

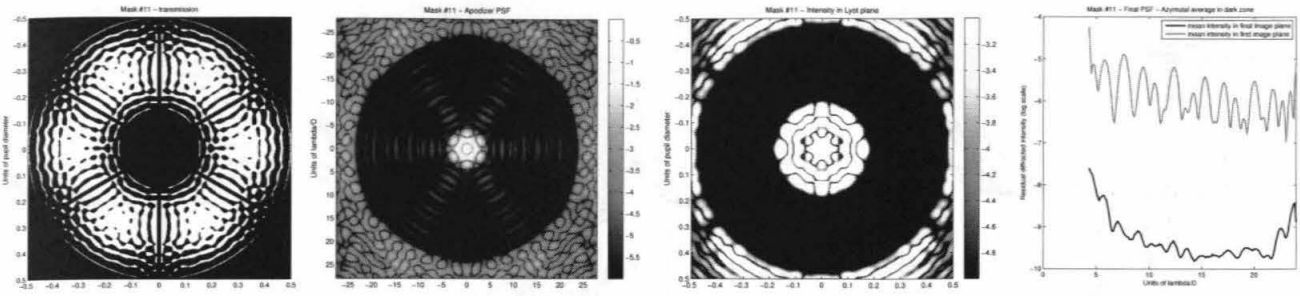

(a) (b) (c) (d)

Figure 5. (a): transmission of mask #11, (b): PSF (first image plane, log scale), (c): residual intensity in Lyot plane (before the Lyot stop has been applied), (d): azymutal average intensity in the first and final image planes (log scale).

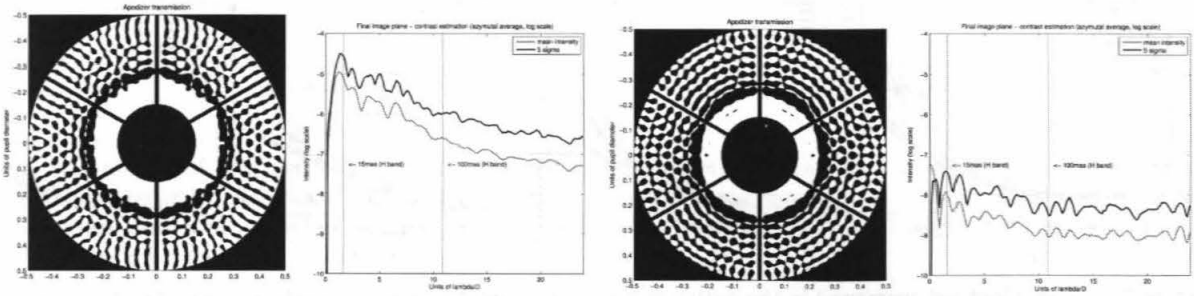

(a) (b)

Figure 6. (a) & (b): Illustration of the AVC coronagraphs. Left: transmission of mask #13 and mask #14; Right: azymutal mean intensity (red) and 5 sigma level (black) in final image planes (log scale). The vertical solid lines show the 15mas and 100mas distance to the star in the H band.

2.3 Apodized vortex coronagraph

The two apodizers numerically optimized for a charge 4 vortex coronagraph - mask #13 and #14 - are shown in Fig.6. The coronagraphs have respectively a 13% and an 8.5% throughput.

Like with the SPLC, the apodizers optimized for the vector vortex have been computed over 512-by-512 points arrays, and the symmetries of the aperture have been used to reduce the effective number of points to 256-by-256, as the transmission only needs to be optimized in one quadrant of the pupil plane. Masks #13 and #14 are otherwise computed as other AVCs.[?,7] The Lyot stop used in these optimizations has a 60% central obscuration, making it twice has large as the E-ELT central obscuration. This is done to maximize the throughput of the coronagraph. As for the SPLC, the outer diameter of the Lyot stop is slightly less than that of the aperture, and the spiders thickness has also been increased.

As observed before the apodizers are formed of an inner highly transmissive ring-like region, surrounded by a mostly zero-transmission region, and a second ring-like region with a medium transmission. This type of apodizer is remarkably similar to the 1D analytical solutions proposed for the charge 4 vector vortex coronagraphs.[9]

While we do not plot here the transmission of an off-axis source, it has already been showed that a 30% central obscuration induces a $3\lambda/D$ IWA, defined as the angular separation for which 50% of the maximum transmitted intensity is found. This represents a significant difference with the IWA of the classical vector vortex coronagraph, which is close to $1.8\lambda/D$ for a charge 4 vortex, but for the current AVC a 35-40% transmission is obtained at $2\lambda/D$ from the star.

3. SENSITIVITY TO LOW-ORDER ABERRATIONS AND CHROMATICITY

An important aspect of the direct imaging problem is the sensitivity of the coronagraphs to wavefront aberrations. Another one is their ability or inability to provide high-contrast in a broad band. We have characterized the impact of low-order aberrations on the contrast created by mask #1-14. For the SP and SPLC we have simulated

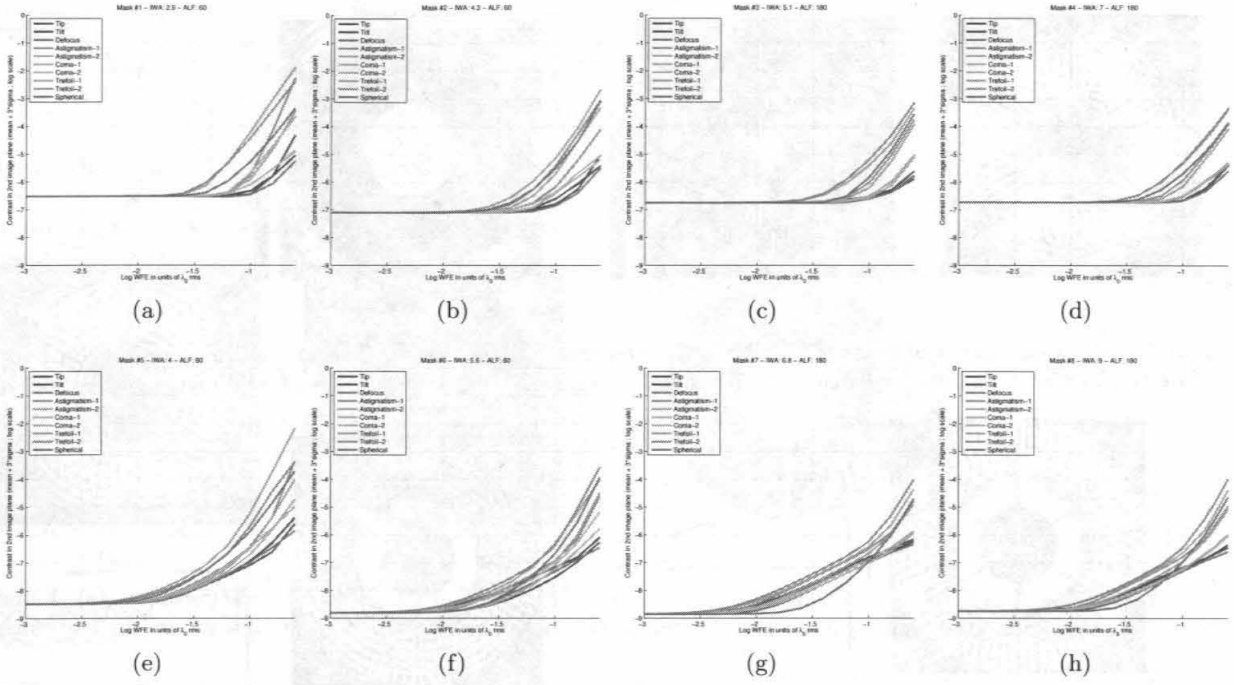

Figure 7. (a)-(g): Contrast measured in the dark zone of the SP coronagraphs for masks #1-#8. The first row correspond to SP designed for a 10^{-6} contrast, and the second row to SP designed for a 10^{-8} contrast. A 10% bandwidth is assumed in the simulations. The x-axis is in units of the log of the wavefront errors, measured in λ_0 RMS. Note that in the H band, 10^{-2} wavefront errors correspond to a 16.5nm RMS aberration. As indicated in each plot, the 10 Zernike modes are represented in colors that follow the visible spectrum of light.

observations in a 10% bandwidth, while we have limited our simulations to monochromatic light for the AVC (mask #13 and #14).

Ten Zernike modes - namely the tip, tilt, defocus, astigmatism, coma, trefoil and spherical aberrations - have been introduced in the simulation, with various amplitudes going from $\lambda_0/1000$ RMS to $\lambda_0/3$ RMS. For the SP and SPLC λ_0 is the central wavelength of the observation bandwidth, while for the AVC λ_0 is the minimum wavelength of the bandwidth (this is done to minimize the chromaticity of the AVC). The amplitude of the Zernike modes is normalized over the aperture of the E-ELT, and not on the apodizer.

Fig.7 illustrates the sensitivity of the SP coronagraphs. The contrast that is plotted is measured in the final image plane.

It appears that SP designed for a 10^{-6} contrast, and which effectively achieve 10^{-7} contrast, are only impacted by aberrations with amplitudes larger than $\lambda_0/30$. The SP designed for a 10^{-8} contrast, and which achieve a 10^{-9} contrast, are impacted by aberrations with smaller amplitudes that range between $\lambda_0/300$ and $\lambda_0/100$.

In both cases the less impacting Zernike modes are the tip, tilt and defocus, while the most impacting modes are the trefoils and the spherical aberration. The IWA for which the mask is designed has an impact on the contrast loss caused by the aberrations, but it only appears for aberrations with large aberrations. For instance mask #1, designed for a $2.9\lambda/D$ IWA, creates a 10^{-4} contrast for $\lambda_0/10$ aberrations, while mask #2-#4, designed for 4.3-$7\lambda/D$ IWA create a 10^{-5} contrast, or lower, for the same amplitude of wavefront errors.

Fig.8 shows aberrated contrast curves for mask #2, with the contrast measured either in the first image plane or in the final image plane. The focal plane mask and the Lyot stop appear to be globally lowering the sensitivity of the SP coronagraph. In particular the focal plane mask does not seem to change the relative impact of the tip and tilt with respect to the other Zernike modes.

Fig.9 illustrates the sensitivity of the SPLC coronagraphs.

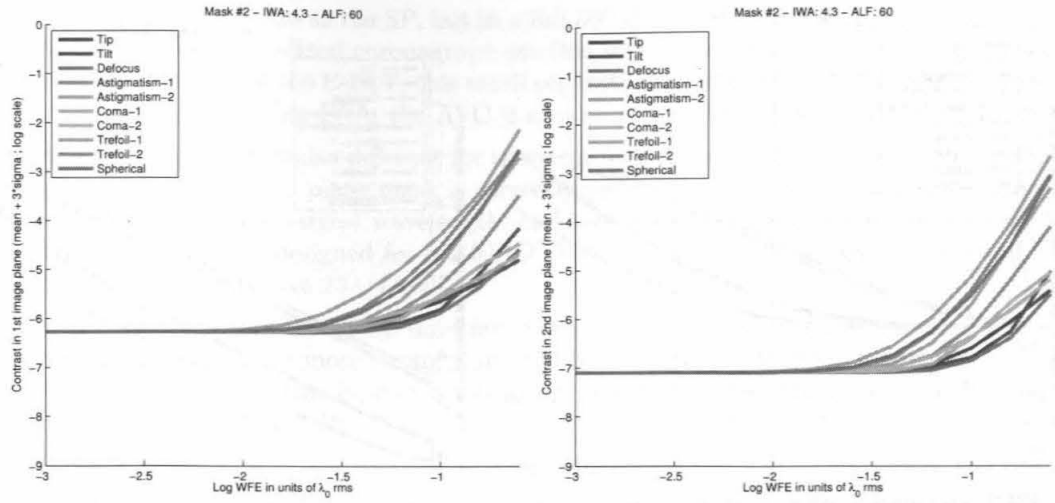

(a) (b)

Figure 8. (a): aberrated contrast for mask #2 measured in the first image plane. (b): aberrated contrast for mask #2 measured in the second image plane. A 10% bandwidth is assumed in the simulations. The x-axis is in units of the log of the wavefront errors, measured in λ_0 RMS. As indicated in each plot, the 10 Zernike modes are represented in colors that follow the visible spectrum of light.

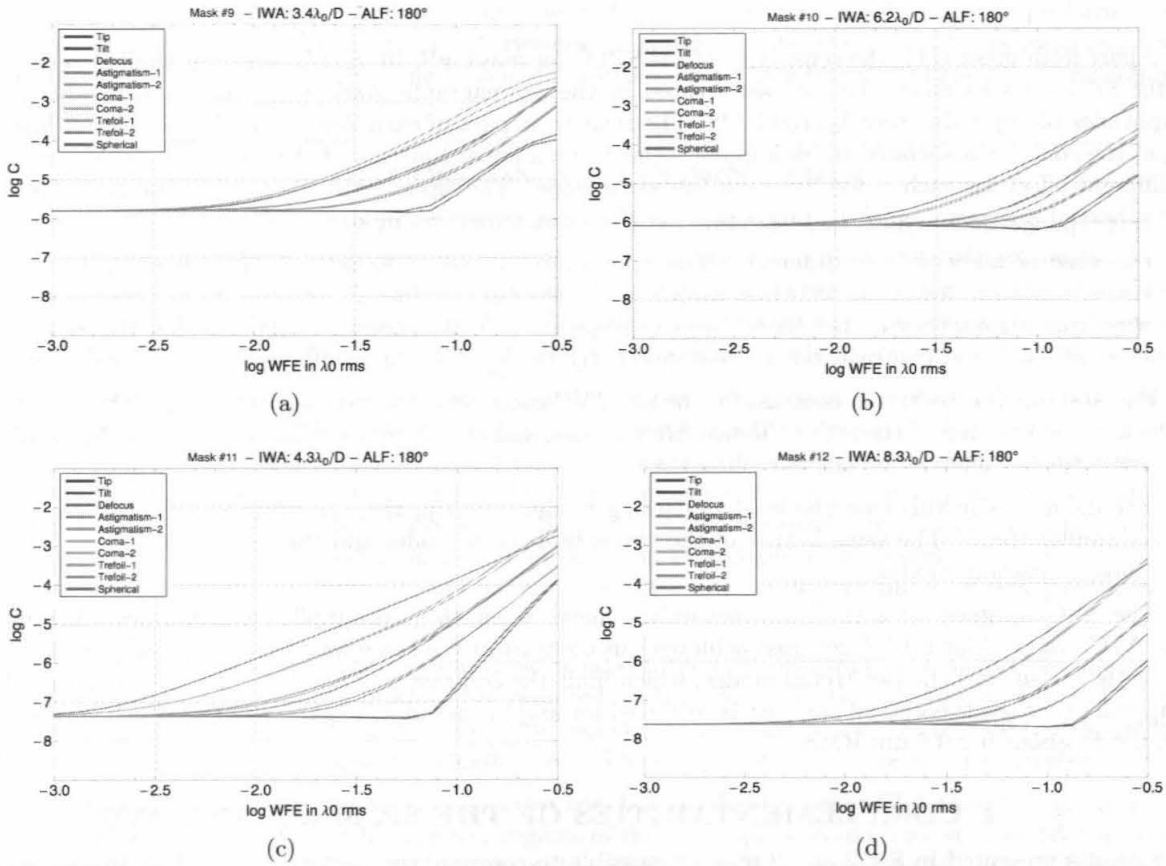

(a) (b)

(c) (d)

Figure 9. (a)-(d): Contrast measured in the dark zone of the SPLC coronagraphs for masks #9-#12. The first row correspond to apodizers designed for a 10^{-6} contrast, and the second row to apodizers designed for a 10^{-8} contrast. A 10% bandwidth is assumed in the simulations. The x-axis is in units of the log of the wavefront errors, measured in λ_0 RMS. As indicated in each plot, the 10 Zernike modes are represented in colors that follow the visible spectrum of light.

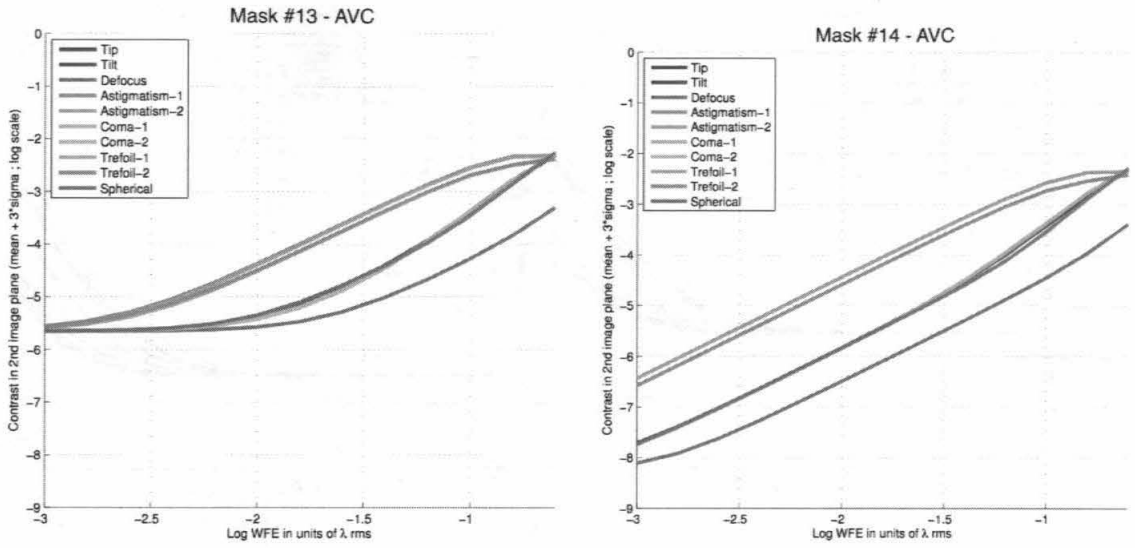

(a) (b)

Figure 10. (a) & (b): Contrast measured in the dark zone of the AVC coronagraphs for masks #13 & #14. A 10% bandwidth is assumed in the simulations. The x-axis is in units of the log of the wavefront errors, measured in λ_0 RMS. As indicated in each plot, the 10 Zernike modes are represented in colors that follow the visible spectrum of light.

Apart from mask #11, the sensitivity of the SPLC for mask #9, 10, and 12 is rather similar to the sensitivity of the SP for masks #1-8: the contrast created by the coronagraphs starts to be impacted by aberrations with amplitudes of approximately $\lambda_0/100$ RMS. The relative impact of each Zernike mode is different, however. The log of the contrast associated to each mode seems to be a linear function of the log of the wavefront errors, with a different offset for each mode but with the same slope. The tip and tilt are the less impacting modes, while the spherical aberration and the two comas are the most impacting modes.

The case of mask #11 is different. The minimum contrast is found for $\lambda_0/1000$ aberration amplitudes. Moreover, while the log of the contrast associated to the tip and the tilt are still linear functions of the log of the wavefront errors, they do not have the same slope as the other modes. It appears that this is the result of a rather small IWA and contrast, but more importantly, of the 10% bandwidth used in the simulation.

Fig.10 shows the aberrated contrast for the two AVC coronagraphs. Here again the log of the contrast appears to be a linear function of the log of the wavefront errors, and the slope is similar for every modes, while an offset differentiates the relative impact of each of them.

The defocus is in this case the least impacting mode. The tip, tilt, spherical and the two comas all follow a very similar trend. The same is true of the two astigmatism modes and the two trefoil modes, which are the four most impacting modes.

The AVC designed for a 10^{-6} contrast only achieves a few 10^{-6} for amplitudes lower than $\lambda/1000 - \lambda/300$. The AVC designed for a 10^{-8} contrast achieves this contrast at the same wavefront errors amplitudes but for the two astigmatism and the two trefoil modes, which limit the contrast to a few 10^{-7}. By extrapolating the curves, it appears that the theoretical contrast is retrieved for amplitudes of $\lambda/10000 - \lambda/3000$, which correspond in the H band to about 0.2-0.5 nm RMS.

4. COMPLEMENTARITIES OF THE SP, SPLC, AND AVC

The results presented in Sec.2 and 3 make it possible to compare the performance and the respective interests of the SP, SPLC, and AVC. The SP coronagraphs are the most robust to wavefront aberrations, and they can be designed to achieve relatively small angular separations of 3-4λ/D, but only in small discovery regions. The SPLC are almost as robust to wavefront aberrations as the SP are. Given the same throughput, they can almost

achieve the same angular separation as the SP, but in a full 360 deg. discovery space instead of a 3 times smaller region. The AVC is the only apodized coronagraph studied in this paper that can achieve a 2-3λ/D angular separation. Given the aperture of the E-ELT, this small separation is obtained at the expense of the throughput. Because of its fundamentally smaller IWA, the AVC is also more sensitive to wavefront aberrations.

The impact of the bandwidth is also different for these coronagraphs. In this regard SP are the least sensitive to chromaticity, as long as the focal plane mask is correctly adjusted. Its physical dimensions must be designed for the IWA corresponding to the largest wavelength, and the OWA corresponding to the smallest wavelength. For instance, mask #1, which is designed for a 2.9λ/D IWA and a 24λ/D, creates a broadband PSF with an effective 3λ/D IWA, and an effective 23λ/D OWA.

The impact of chromaticity of the SPLC does not seem to be much more significant than it is with the SP, although the contrast appears to be more strongly affected by it for masks designed for smaller IWA and smaller contrast. It should be noted that this type of coronagraph is known to be chromatic, and that masks #9-#12 have been optimized monochromatically.

While we did not show plots of the contrast in a broadband for the AVC, this aspect has been studied in the past[10] for a 20% centrally obstructed aperture with 0.5% thick spiders with a four-fold symmetry. For a 20% band it resulted in a 10^{-8} contrast instead of a 10^{-9} contrast. Preliminary results not shown in the current paper indicate that chromaticity may be a more important concern for the E-ELT aperture, which has a 30% central obscuration and 1.3% thick spiders with a six-fold symmetry. As for the SPLC, the AVC is known to be a chromatic coronagraph, and the current optimization of the apodizer is monochromatic.

These properties make these three solutions quite complementary as observations that require the smallest possible angular separation can be achieved with the AVC, while observations that can be performed with a medium resolution can use a SP or an SPLC. Besides, it could be interesting for the astronomers and the telescope operators to be able to adjust the choice of the coronagraph as a function of the observing conditions, or the required bandwidth.

5. DISCUSSION AND CONCLUSION

We have reviewed in this paper three possible types of apodized coronagraphs designed for the aperture of the E-ELT. The objective of the PCS instrument is a $10^{-8} - 10^{-9}$ contrast. Given the different masks presented here, this contrast can be achieved at various IWA and throughput. The closest angular separation - 2-3 λ/D - is given by the apodized vortex coronagraph. With its current implementation this coronagraph achieves 8.5% throughput. This is mostly due to the spiders thickness of the E-ELT. Without spiders, the through

Several possible solutions are currently being studied to increase the throughput of the AVC, and of the other apodized coronagraphs as well. One is to remap the pupil using the active correction of aperture discontinuities (ACAD) proposed by Pueyo & Norman.[15] Using two deformable mirrors (DM), this technique changes the energy density of the pupil to make the spiders thinner. This is a lossless technique similar to phase induced amplitude apodization (PIAA[16]). A second possibility would be to use phase apodizers instead of amplitude apodizers. New techniques have been developed to induce phase shifts in broadband using layers of liquid crystals. In all cases, an AVC would require a dual DM system to correct for amplitude and phase aberrations[17] since this coronagraph is quite sensitive to wavefront errors.

While the SP and SPLC would benefit from these advances, these coronagraphs can already be manufactured using existing techniques. They can produce the required contrast for PCS, though only at 4λ/D at best for a 25% throughput. This is done with the SP in narrow regions of the image plane. Decreasing the throughput or the OWA makes it possible to work with a smaller IWA. These trade-offs are currently investigated.

Current SPLC designs create the required contrast too, but for slightly larger IWA than SP, and in a full 360 deg. region. SPLC creating contrast in narrower regions of the image plane could have smaller IWA as well, and the same considerations of throughput and OWA apply as with the SP. These trade-offs will be investigated in the near future.

The sensitivity to aberrations of the SP coronagraph and the SPLC makes them good candidates for instruments that only rely on the adaptive optic system of the telescope. For instance, a 25% throughput, 3λ/D SP

would achieve $10^{-6} - 10^{-7}$ contrast in symmetric regions of the image planes, and a 25% throughput, $3.4\lambda/D$ SPLC would achieve 10^{-6} contrast in a full 360 deg. region.

SP could in particular be used to provide the high-contrast imaging mode of HARMONI. The current optical design of this instrument does not include an atmospheric dispersion corrector (ADC), which precludes the use of any coronagraphs that relies on a focal plane mask to create high-contrast.

It will be necessary to simulate realistic aberration patterns to try and characterize more accurately the performance of all these coronagraphs. It will also be interesting to characterize their performance in various bandwidths. Other aberrations must be taken into account to estimate the performance of these instruments. Such aberrations include the standard deviation of the mirrors reflectivity, and the random absence of several segments each night. While these aberrations may not limit the performance of the coronagraphic modes of the first light instruments, they will be an important issue for PCS. ACAD may be used to circumvent these issues, but the required stroke may be too high to achieve the required contrast. An adaptive apodizer using a micro-mirror array with 10^6 elements could also be an efficient solution to this problem. Technological developments will be required in both cases.

REFERENCES

[1] Kasper, M., Verinaud, C., and Mawet, D., "Roadmap for PCS, the Planetary Camera and Spectrograph for the E-ELT," in [*Proceedings of the Third AO4ELT Conference*], Esposito, S. and Fini, L., eds. (Dec. 2013).

[2] Kasdin, N. J., Vanderbei, R. J., Spergel, D. N., and Littman, M. G., "Extrasolar Planet Finding via Optimal Apodized-Pupil and Shaped-Pupil Coronagraphs," *The Astrophysical Journal* **582**, 1147–1161 (Jan. 2003).

[3] Carlotti, A., Vanderbei, R., and Kasdin, N. J., "Optimal pupil apodizations of arbitrary apertures for high-contrast imaging," *Optics Express* **19**, 26796 (Dec. 2011).

[4] Aime, C., Soummer, R., and Ferrari, A., "Total coronagraphic extinction of rectangular apertures using linear prolate apodizations," *Astronomy & Astrophysics* **389**, 334–344 (July 2002).

[5] Soummer, R., "Apodized Pupil Lyot Coronagraphs for Arbitrary Telescope Apertures," *The Astrophysical Journal* **618**, L161–L164 (Jan. 2005).

[6] Rouan, D., Riaud, P., Boccaletti, A., Clénet, Y., and Labeyrie, A., "The Four-Quadrant Phase-Mask Coronagraph. I. Principle," *Publications of the Astronomical Society of the Pacific* **112**, 1479–1486 (Nov. 2000).

[7] Carlotti, A., "Apodized phase mask coronagraphs for arbitrary apertures," *Astronomy & Astrophysics* **551**, A10 (Mar. 2013).

[8] Mawet, D., Riaud, P., Absil, O., and Surdej, J., "Annular Groove Phase Mask Coronagraph," *The astrophysical Journal* **633**, 1191–1200 (Nov. 2005).

[9] Mawet, D., Pueyo, L., Carlotti, A., Mennesson, B., Serabyn, E., and Wallace, J. K., "Ring-apodized Vortex Coronagraphs for Obscured Telescopes. I. Transmissive Ring Apodizers," *The Astrophysical Journal Supplement* **209**, 7 (Nov. 2013).

[10] Carlotti, A., Pueyo, L., and Mawet, D., "Apodized phase mask coronagraphs for arbitrary apertures. II. Comprehensive review of solutions for the vortex coronagraph," *Astronomy & Astrophysics* **566**, A31 (June 2014).

[11] Vanderbei, R. J., Spergel, D. N., and Kasdin, N. J., "Circularly Symmetric Apodization via Star-shaped Masks," *The Astrophysical Journal* **599**, 686–694 (Dec. 2003).

[12] Macintosh, B. A., Graham, J. R., Palmer, D. W., Doyon, R., Dunn, J., Gavel, D. T., Larkin, J., Oppenheimer, B., Saddlemyer, L., Sivaramakrishnan, A., Wallace, J. K., Bauman, B., Erickson, D. A., Marois, C., Poyneer, L. A., and Soummer, R., "The Gemini Planet Imager: from science to design to construction," in [*Society of Photo-Optical Instrumentation Engineers (SPIE) Conference Series*], *Society of Photo-Optical Instrumentation Engineers (SPIE) Conference Series* **7015** (July 2008).

[13] Beuzit, J.-L., Feldt, M., Dohlen, K., Mouillet, D., Puget, P., Wildi, F., Abe, L., Antichi, J., Baruffolo, A., Baudoz, P., Boccaletti, A., Carbillet, M., Charton, J., Claudi, R., Downing, M., Fabron, C., Feautrier, P., Fedrigo, E., Fusco, T., Gach, J.-L., Gratton, R., Henning, T., Hubin, N., Joos, F., Kasper, M., Langlois, M., Lenzen, R., Moutou, C., Pavlov, A., Petit, C., Pragt, J., Rabou, P., Rigal, F., Roelfsema, R., Rousset,

G., Saisse, M., Schmid, H.-M., Stadler, E., Thalmann, C., Turatto, M., Udry, S., Vakili, F., and Waters, R., "SPHERE: a planet finder instrument for the VLT," in [*Society of Photo-Optical Instrumentation Engineers (SPIE) Conference Series*], *Society of Photo-Optical Instrumentation Engineers (SPIE) Conference Series* **7014** (Aug. 2008).

[14] Martinez, P., Dorrer, C., Aller Carpentier, E., Kasper, M., Boccaletti, A., Dohlen, K., and Yaitskova, N., "Design, analysis, and testing of a microdot apodizer for the Apodized Pupil Lyot Coronagraph," *Astronomy & Astrophysics* **495**, 363–370 (Feb. 2009).

[15] Pueyo, L. and Norman, C., "High-contrast Imaging with an Arbitrary Aperture: Active Compensation of Aperture Discontinuities," *The Astrophysical Journal* **769**, 102 (June 2013).

[16] Guyon, O., "Phase-induced amplitude apodization of telescope pupils for extrasolar terrestrial planet imaging," *Astronomy & Astrophysics* **404**, 379–387 (June 2003).

[17] Pueyo, L. and Kasdin, N. J., "Polychromatic Compensation of Propagated Aberrations for High-Contrast Imaging," *The Astrophysical Journal* **666**, 609–625 (Sept. 2007).